AIP
CONFERENCE
PROCEEDINGS 275

ATOMIC PHYSICS 13

THIRTEENTH INTERNATIONAL CONFERENCE ON ATOMIC PHYSICS

MUNICH, GERMANY 1992

EDITORS:
H. WALTHER
T. W. HÄNSCH
B. NEIZERT
MAX PLANCK INSTITUTE
FOR QUANTUM OPTICS
GARCHING, GERMANY
AND
LUDWIG MAXIMILIAN UNIVERSITY
MUNICH, GERMANY

AIP
American Institute of Physics
New York

QUANTUM PHENOMENA IN ATOMIC COOLING

C. Cohen-Tannoudji
Collège de France and Laboratoire de Spectroscopie Hertzienne
de l'E.N.S.*, 24 rue Lhomond, F-75231 Paris Cedex 05, France

ABSTRACT

New laser cooling mechanisms, more efficient than Doppler cooling, allow one to reach new regimes where the quantum nature of the translational degrees of freedom of an atom can no longer be ignored. This paper reviews a few examples of quantum phenomena observable on laser cooled atoms : quantization of atomic motion in an optical potential, de Broglie wavelengths larger than the wavelength of the laser used to cool the atoms. New theoretical approaches to these problems will be also briefly mentioned.

INTRODUCTION

Two types of variables must be considered for specifying the state of an atom. First, internal variables, which refer to the state of the electrons in the center of mass rest frame. Quantum mechanics is essential for describing such an internal motion and this explains why atomic physics, which deals with the internal structure of atoms, has played a central role in the birth of quantum mechanics. The other variables, generally called external variables, are the position $\vec{R}$ and the momentum $\vec{P}$ of the atomic center of mass. The total mass M of atom being much larger than the electron mass m, the de Broglie wavelengths associated with the center of mass motion are generally extremely small and this explains why a semiclassical treatment of external variables is most often sufficient.

During the last few years, laser cooling and trapping methods have given us a much better control of external variables[1], and new regimes are now reached where the quantum nature of external variables can no longer be ignored. Quantum phenomena become visible on laser cooled atoms. This paper is devoted to a review of such effects and to a discussion of some new theoretical approaches to these problems.

We first recall a few basic results concerning light shifts of atomic ground states and photon absorption rates from these states, since it turns out that these effects play an important role in the recent developments of laser cooling. Then, we have chosen to discuss two extreme situations where quantum phenomena observable on external variables can be associated, respectively, with position-dependent effects and momentum dependent effects. In the first case,

*Laboratoire associé au CNRS et à l'Université Pierre et Marie Curie.

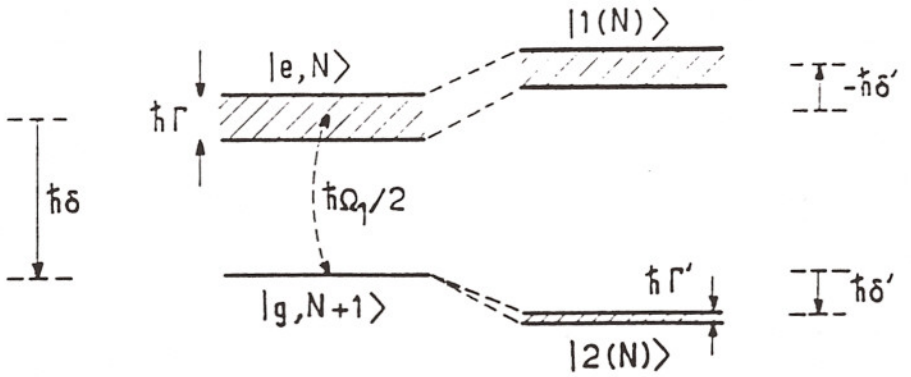

Fig. 1 : Two uncoupled states of the atom+laser photons system $|g, N+1\rangle$ and $|e, N\rangle$ (left part of the figure) giving rise to the two dressed states $|1(N)\rangle$ and $|2(N)\rangle$ when the atom-laser coupling is taken into account (right part). δ' and Γ' are, respectively, the light shift of the ground state and the photon absorption rate from this state.

we show how position-dependent light shifts and position-dependent absorption rates can give rise to a cooling mechanism, called now Sisyphus cooling, which is so efficient that quantization of atomic motion in an optical potential well can be observed. The second example which will be discussed uses Doppler effect on Raman type transition for achieving a very efficient selection in momentum space. Combining such a velocity selection with optical pumping in velocity space, one can realize subrecoil schemes which lead to atomic de Broglie wavelengths larger than the wavelength of the laser which is used to cool the atoms. In connection with these experiments, we will also describe a Monte-Carlo simulation of the cooling process which is typical of new theoretical approaches which are presently being explored and which seem quite promising. Finally, let us mention that we will not discuss here atomic interferometry and atom optics, although they are obviously related to the wave nature of atomic motion. We refer the reader to other review papers of this volume[2].

LIGHT SHIFTS AND PHOTON ABSORPTION RATES

A very simple way for introducing these effects is to use a dressed atom approach[3]. We consider a two-level atom, with an excited state e and a ground state g separated by an energy internal $\hbar\omega_A$, coupled to a single mode laser field, with frequency ω_L. The left part of Fig. 1 represents two uncoupled states of thc atom+laser photons system : the state $|e, N\rangle$ (atom in e in the presence of N laser photons) and the state $|g, N+1\rangle$ (atom in g in the presence of $N+1$ laser photons). These two states are separated by an energy interval $\hbar\delta$, where :

$$\delta = \omega_L - \omega_A \tag{1}$$

is the detuning between the laser frequency ω_L and the atomic frequency ω_A. In Fig. 1, the level $|e, N\rangle$ is represented with a width $\hbar\Gamma$, where $\Gamma = 1/\tau_R$ is the inverse of the radiative lifetime τ_R of the excited state. Such a natural width Γ describes the unstability of e due to spontaneous emission. The right part of Fig. 1 represents the coupled, or dressed states, which originate from the previous unperturbed states when the atom-laser coupling V_{AL} is taken in account. The atom in g can absorb one laser photon and jump into e. It follows that the two states $|g, N+1\rangle$ and $|e, N\rangle$ are connected by V_{AL}. We have :

$$\langle e, N|V_{\mathrm{AL}}|g, N+1\rangle = \hbar\Omega_1/2 \tag{2}$$

where Ω_1 is the Rabi frequency characterizing the atom-laser coupling. Under the effect of such a coupling, the two states $|g, N+1\rangle$ and $|e, N\rangle$ repel each other and give rise to the two dressed states $|1(N)\rangle$ and $|2(N)\rangle$. The light shift $\hbar\delta'$ of the ground state is nothing but the energy displacement of $|g, N+1\rangle$ due to the coupling V_{AL} (see Fig. 1). The state $|e, N\rangle$ undergoes an opposite shift $-\hbar\delta'$. Note also that, as a consequence of the contamination of $|g, N+1\rangle$ by $|e, N\rangle$ due to V_{AL}, a small part of the unstability of $|e, N\rangle$ is transferred to $|g, N+1\rangle$. The dressed state $|2(N)\rangle$ gets a finite width $\hbar\Gamma'$ (see Fig. 1). The parameter Γ' can be interpreted as the departure rate from $|g, N+1\rangle$ due to V_{AL}, i.e. as the photon absorption rate from g. Similarly, the contamination of $|e, N\rangle$ by $|g, N+1\rangle$ slightly reduces the width $\hbar\Gamma$ of e.

Simple perturbative expressions may be given for δ' and Γ' in the limit :

$$|\delta| \gg \Gamma, \Omega_1 \tag{3}$$

One finds :

$$\delta' = \frac{\Omega_1^2}{4\delta} \tag{4a}$$

$$\Gamma' = \Gamma\frac{\Omega_1^2}{4\delta^2} = \frac{\Gamma}{\delta}\delta' \tag{4b}$$

Equations (4) show that both the light shift and the photon absorption rate are proportional to Ω_1^2, i.e. to the laser intensity I_L. It is clear also from (4a) that the light shift δ' has the same sign as the detuning δ. It is positive for $\omega_L > \omega_A$, and negative for $\omega_L < \omega_A$ (which is the case for Fig. 1). The comparison of (4a) and (4b) clearly shows also that, by varying the detuning δ, one can control the relative values of Γ' and δ'. For large detunings ($|\delta| \gg \Gamma$), Γ' is much smaller than δ', by a factor Γ/δ.

Actually, light shifts were first introduced for an atom having several ground state sublevels[4,5], and their experimental observation[5-7] predates the use of lasers in atomic physics. They were induced by the light coming from a discharge lamp (this is why they were called "Lamp shifts" by Alfred Kastler, in

a word play indicating their origin and their analogy with the Lamb shift). The fact that the light shifts depend on the polarization of the light beam and vary from one ground state sublevel to the other was essential for their observation. Because of the length of relaxation times in atomic ground states, magnetic resonance curves in these states are very narrow, and even if the light shifts of two ground state sublevels differ only by a few Hertz, such an effect can be easily detected by a shift of the magnetic resonance curve[5,6]. During the last few years, it has been realized that optical pumping and light shifts can play also an important role in the dynamics of the external degrees of freedom of an atom having several ground state sublevels. New laser cooling mechanims, based on these effects and much more efficient than Doppler cooling, have been discovered[8]. We discuss, in the next section, an example of such a situation.

QUANTIZATION OF ATOMIC MOTION IN AN OPTICAL POTENTIAL WELL

We first briefly recall the principle of $1D$ Sisyphus cooling which results from strong correlations which can appear between the spatial modulation of optical pumping rates between two ground state Zeeman sublevels and the spatial modulation of the light shifts of these sublevels. These correlations result in the fact that the moving atom moves up in potential hills more than down, as did Sisyphus in the Greek mythology.

We consider the specific example of a $J_g = 1/2 \longrightarrow J_e = 3/2$ atomic transition, the various Zeeman components of the optical line and the corresponding relative transition probabilities being shown in Fig. 2a. The laser configuration is supposed to consist of two counterpropagating laser waves having the same amplitude, a negative detuning ($\omega_L < \omega_A$) and orthogonal linear polarizations. Fig. 2b shows the resulting polarization of the total field which changes, every $\lambda/8$, from linearly polarized to circularly polarized and vice versa. The light shifts of the two ground state Zeeman sublevels $g_{\pm 1/2}$ are negative and oscillate in space, as shown in Fig. 2c, since the light shift of $g_{+1/2}$ is three times larger (in absolute value) that the light shift of $g_{-1/2}$ in the places where the polarization is σ^+ (see the transition probabilities of Fig. 2a), the reverse being true in the places where the polarization is σ^-. We denote U_0 the depth of the optical potential wells resulting from such a modulation. It is clear also that optical pumping tends to transfer atoms from the highest Zeeman sublevel to the lowest one since σ^+ (respectively, σ^-) optical pumping tends to accumulate atoms in $g_{+1/2}$ (respectively, $g_{-1/2}$). Consider now an atom moving to the right and starting from the bottom of a valley (Fig. 2c). If its velocity v is such that $v\tau_P \sim \lambda$, where τ_P is the optical pumping time which is inversely proportional to the photon absorption rate Γ', the atom has enough time to climb the potential hill and to reach the top of this hill where it has the highest probability of being optically pumped to the bottom of a potential valley. Part of its kinetic energy

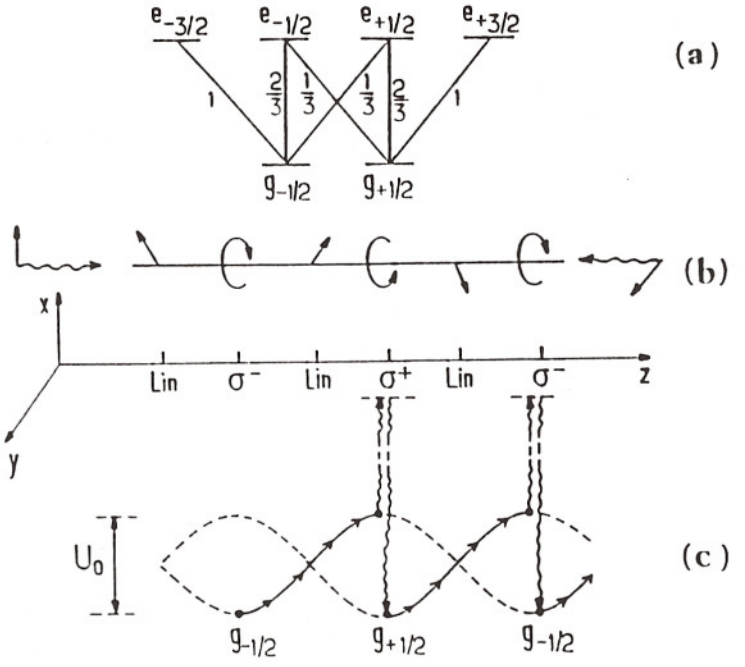

Fig. 2 : Principle of Sisyphus cooling. (a) Relative transition probabilities for a $J_g = 1/2 \longrightarrow J_e = 3/2$ transition. (b) Polarization of the laser field obtained by adding the electric fields of two counterpropagating waves with orthogonal linear polarizations. (c) Spatial modulation of the light shifts of the two ground state sublevels. Because of the correlated spatial modulation of optical pumping rates, the moving atom moves up in potential hills more than down.

has been transformed into potential energy, which is then dissipated by the fluorescence photon which has an energy higher than the absorbed laser photon. From there, the same sequence can be repeated. On the average, the moving atom is running up the hills more than down and its total energy decreases by discontinuous steps, on the order of U_0, until it gets trapped in the potential wells of Fig. 2c. Its kinetic energy is then on the order of U_0, so that, using (4b) :

$$k_B T_S \sim U_0 \sim \hbar \frac{\Omega_1^2}{|\delta|} \tag{5}$$

where T_S is the equilibrium temperature associated with Sisyphus cooling. Such a qualitative prediction is confirmed by more quantitative calculations leading to analytical expressions for the friction coefficient and the momentum diffusion coefficient[9]. Numerical integrations of optical Bloch equations have been also performed for more complex atomic transitions[10]. The fact that T_S is proportional to the laser intensity $I_L \sim \Omega_1^2$ and inversely proportional to the detuning $|\delta|$ is in quite good agreement with experimental observations[11].

The proportionality of T_S to I_L cannot remain valid for arbitrary low intensity. There are quantum limits to Sisyphus cooling which are not correctly described by the semiclassical treatment leading to (5). Physically, the decrease

of potential energy after each optical pumping cycle, which is on the order of U_0, must be larger than the increase of kinetic energy, due to the recoil E_R of the absorbed or emitted photon :

$$E_R = \hbar^2 k^2 / 2M \tag{6}$$

This shows that there is a threshold for U_0, below which Sisyphus cooling no longer works, and the smallest temperatures which can be achieved by such a cooling scale as E_R and not as $\hbar\Gamma$, as is the case for Doppler cooling. In order to determine more precisely the optimum of Sisyphus cooling, a full quantum treatment has been worked out[12], where the quantum equations of motion are solved numerically. For Cesium, one finds that the smallest achievable root mean square momentum is on the order of $p_{\rm rms} \simeq 5.5\hbar k$, corresponding to a velocity of 1.5 cm/s, these values being reached for $U_0 \simeq 95 E_R$ and for $|\delta| \gg \Gamma$. For these values, the atom oscillates several times in the bottom of the optical potential wells of Fig. 2c, before undergoing an optical pumping cycle. Its oscillation frequency $\Omega_{\rm osc}$, which is proportional to $\sqrt{I_L/|\delta|}$, becomes larger than the photon absorption rate $\Gamma' \sim 1/\tau_P$, which is proportional to I_L/δ^2 :

$$\Omega_{\rm osc} \gg 1/\tau_P \tag{7}$$

Condition (7) corresponds to an interesting unusual situation where external times, $2\pi/\Omega_{\rm osc}$, associated with the motion of the center of mass, become shorter than internal times, on the order of τ_P. This explains the failure of semiclassical treatments where internal variables are adiabatically eliminated, leading to a Fokker-Planck equation for external variables.

New theoretical methods[13] have been developed for describing laser cooling in the regime $\Omega_{\rm osc}\tau_P \gg 1$, where, as a result of condition $|\delta| \gg \Gamma$, light shifts are much larger than optical pumping rates. The equation of motion for the ground state density matrix σ_g (including both internal and external degrees freedom) can be written :

$$\frac{\mathrm{d}}{\mathrm{d}t}\sigma_g = \frac{1}{i\hbar}\left[H_{\rm eff}(Z) + \frac{P^2}{2M}, \sigma_g\right] + \text{Optical pumping terms} \tag{8}$$

where $H_{\rm eff}$ is the effective Hamiltonian describing light shifts in the ground state manifold, and where Z and P are the position and momentum operators for the center of mass. In the limit of large light shifts, one can, in a first step, neglect the second line of Eq. (8), since optical pumping terms are proportional to Γ' and are thus much smaller than $H_{\rm eff}(Z)$, which is proportional to δ'. The first line of Eq. (8) describes a pure Hamiltonian evolution of the atom in the optical bipotential of Fig. 2c. The diagonalisation of the corresponding Hamiltonian gives a series of vibrational levels $v = 0, 1, 2...$, which are actually energy bands because

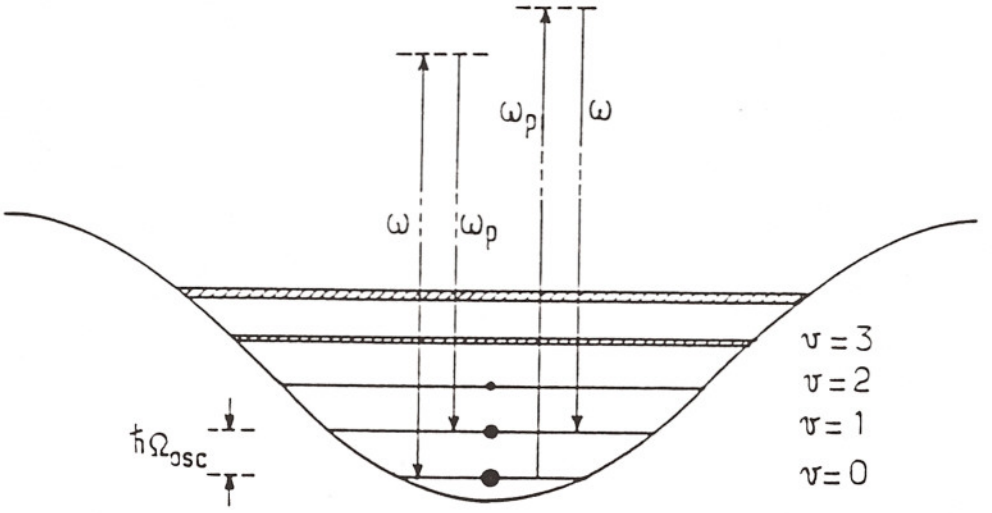

Fig. 3 : First energy bands corresponding to one of the two potential curves of Fig. 2c. The energy interval between the two deepest bands is $\hbar\Omega_{osc}$. The solid circles give an idea of the populations of the bands. The vertical arrows describe the stimulated Raman processes at the origin of the two lateral resonances of the experimental spectrum of Fig. 4b.

of the periodicity of the optical potentials. Figure 3 gives a sketch of such bands corresponding to the optical potential of one of the two Zeeman sublevels $g_{\pm 1/2}$. The lowest bands are very narrow because of the smallness of the tunnel effect between two adjacent potential wells and the energy internal between the two deepest bands is nothing but $\hbar\Omega_{osc}$ because of the quasi-harmonic character of the potential well. The second step of the calculation consists in taking into account the effect of optical pumping between different energy bands or inside a given band. Condition (7) means that the radiative width of the energy bands of Fig. 3, due to optical pumping, is small compared to the energy intervals between bands, so that they remain well resolved. Such a condition (supplemented by symmetry considerations) allows one to neglect any " non secular" coupling between diagonal and off diagonal elements of the density matrix and to describe the whole process in terms just of transition rates between different vibrational levels (or bands) $|v\rangle$. More precisely, one gets :

$$\frac{\mathrm{d}}{\mathrm{d}t}\Pi_v = -\sum_{v' \neq v} \Gamma_{v \to v'} \Pi_v + \sum_{v' \neq v} \Gamma_{v' \to v} \Pi_{v'} \tag{9}$$

where Π_v is the population of level v and where $\Gamma_{v \to v'}$ is the optical pumping rate from v to v'. Since all $\Gamma_{v \to v'}$ are proportional to Γ', the steady state populations Π_v^{st} are independent of Γ', and one can derive in this way universal laws for the temperature[14], relating T/T_R, where $T_R = E_R/k_B$, to a single parameter U_0/E_R.

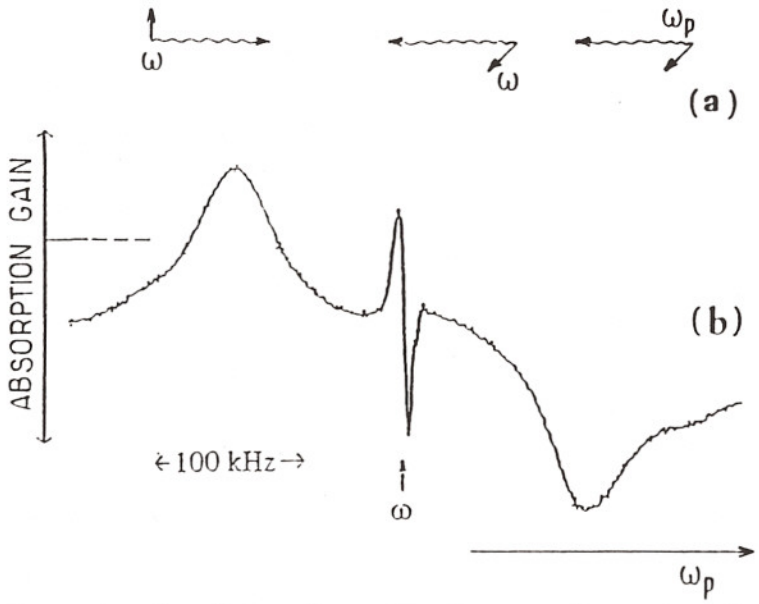

Fig. 4 (a) One-dimensional molasses formed by two counterpropagating pump waves ω with orthogonal linear polarizations. The probe wave ω_P has the same linear polarization as the copropagating pump wave.

(b) Probe absorption spectrum plotted versus ω_P. The signal is typically 10 % of the probe intensity.

EXPERIMENTAL OBSERVATION OF QUANTIZATION OF ATOMIC MOTION

Experimental evidence has been recently obtained for the quantization of atomic motion represented in Fig. 3[15,16]. We will briefly describe here the first experiment[15] using stimulated Raman spectroscopy, since the second one[16] using fluorescence spectroscopy, is discussed in another paper of this volume (by Rolston et al). A one-dimensional molasses is first obtained as follows. Starting from Cesium atoms cooled and trapped in a $3-D$ magneto-optical trap, the inhomogeneous magnetic field of the trap is switched off and the intensity of each trapping beam is reduced from 5 mW/cm^2 to about 0.1 mW/cm^2, while a pump wave of frequency ω made of two counterpropagating waves having orthogonal linear polarizations is switched on (Fig. 4a). The $1-D$ molasses which is achieved in such a transient way (the atomic density decreases with a time constant of 5-50 ms) is then probed by monitoring the transmitted intensity of a weak traveling probe wave of frequency ω_P making a 3° angle with the pump wave. Figure 4b gives an example of experimental probe absorption spectrum plotted versus ω_P and corresponding to the case where the probe wave and the copropagating pump wave have parallel linear polarizations.

The two lateral resonances have a straightforward interpretation in terms of stimulated Raman processes between the vibrational levels of Fig. 3. For the experimental condition considered here, most of the atomic population is con-

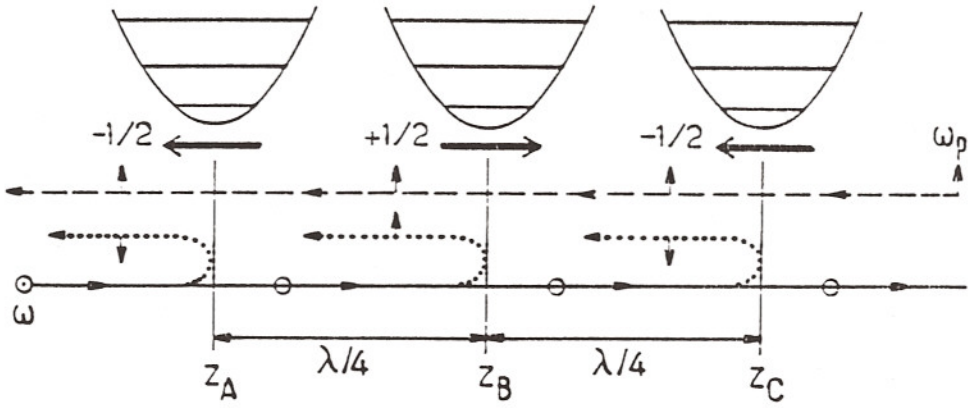

Fig. 5 : Interpretation of the central narrow resonance of Fig. 4b. The pump wave ω coming from the left (solid line) is backscattered by the magnetization grating (thick arrows) produced by the modulated optical pumping due to the interference between the pump and probe waves. The backscattered waves (dotted lines) undergo a (Faraday) rotation of polarization and can interfere with the probe wave ω_P coming from the right (dashed line).

centrated in the first 3 vibrational levels $v = 0, 1, 2$ (the size of the solid circles of Fig. 3 gives an idea of these populations). Starting from the lowest level $v = 0$, the atom can absorb one pump photon ω and make a stimulated emission of one probe photon $\omega_P = \omega - \Omega_{\text{osc}}$ which puts it in $v = 1$ (vertical arrows in the left part of Fig. 3). This explains the lateral resonance in the left part of Fig. 4b which corresponds to an amplification of the probe. The atom can also absorb first from $v = 0$ a probe photon $\omega_P = \omega + \Omega_{\text{osc}}$ and then make a stimulated emission of a pump photon ω which puts it into $v = 1$ (vertical arrows in the right part of Fig. 3). This explains the resonance in the right part of Fig. 4b corresponding to an absorption of the probe. Other experimental curves have been also obtained, showing Raman resonances $\Delta v = 2$. The Raman spectrum of Fig. 4 thus provides an experimental evidence for the existence of quantized energy levels of a neutral atom in an optical field and allows one to measure Ω_{osc}. We refer the reader to ref. [15] for a more detailed discussion concerning the positions and the widths of the Raman resonances of Fig. 4. We just mention here that, from the measured value of Ω_{osc} and from the value of the Cesium mass M, one can estimate the spatial extent $\left[(2\hbar/M\Omega_{\text{osc}})^{1/2}\right]$ of the ground state wave function to be on the order of $\lambda/25$, which corresponds to a very strong spatial localization and is at the origin of an important Lamb-Dicke narrowing of the Raman lines[15]. Note also that a large fraction of the atomic population is optically pumped in the $v = 0$ states which are minimum uncertainty states.

We will conlcude this section by interpreting the narrow central structure of Fig. 4. Because of the interference between the pump and probe waves, the intensity of the total field "seen" by the atoms has a component modulated at $\omega - \omega_P$. The corresponding modulation of optical pumping results in a modulation $\delta\Pi_v$ and $\delta\vec{M}_v$ of the population and magnetization of level v. Because atoms

respond with a finite time constant τ_P (optical pumping time) to any variation of the light intensity, $\delta\Pi_v$ and $\delta\vec{M}_v$ have an amplitude and a phase which vary resonantly with $\omega - \omega_P$ in an interval of width $1/\tau_P$ around $\omega - \omega_P = 0$. The thick arrows of Fig. 5 represent the $\delta\vec{M}_v$ corresponding to three successive potential wells located in z_A, z_B, z_C and separated by $\lambda/4$. Since two successive wells correspond to opposite magnetic quantum numbers $\pm 1/2$ (see also fig. 2c), the $\delta\vec{M}_v$ form an "antiferromagnetic" grating (thick arrows of Fig. 5). Consider now the pump wave, counterpropagating with the probe wave and coming from the left in Fig. 5. This pump wave is backscattered by the grating formed by the $\delta\vec{M}_v$ and one can show that such a backscattered wave (dotted line) has the same frequency, the same wave vector and the same polarization as the probe wave coming from the right in Fig. 5 (dashed line). These two waves, the backscattered pump wave and the probe wave, can thus interfere and this is the origin of the central resonance of Fig. 4. Note that the backscattering by the $\delta\vec{M}_v$ occurs with a rotation of polarization, as in the Faraday effect. This explains why, although the counterpropagating pump and probe waves have orthogonal polarizations (see Fig. 5), the backscattered pump wave has a component of polarization parallel to that of the probe wave. One could think also, at first sight, that the waves backscattered by two successive planes of atoms, separated by $\lambda/4$, interfere destructively because they differ by an optical path $2 \times (\lambda/4) = \lambda/2$. But this change of sign, due to the spatial propagation, is compensated for by the change of sign of the rotation of polarization due to the alternate signs of the $\delta\vec{M}_v$. Finally, it is clear that only localized states, with a small value of v and a small spatial extent Δz_v, can give rise to a backscattered wave since, otherwise, there would be destructive interferences between the waves backscattered by the right part and the left part of the wave function associated with level v. For such localized states, τ_P is very long, because of the Lamb-Dicke effect, and this explains why the central resonance of Fig. 4 is so narrow. To sum up, one can say that the central resonance of Fig. 4 demonstrates the existence of a large scale spatial order of localized atoms, presenting some analogy with an antiferromagnetic medium.

MOMENTUM - DEPENDENT EFFECTS AND SUBRECOIL COOLING

We discuss now subrecoil cooling schemes, applicable to Λ-type atomic transitions, and leading to large atomic de Broglie wavelengths, larger than the wavelength of the cooling laser. The interest of Λ-type transitions is that stimulated Raman processes can take place between the two lower sublevels of the transition which are generally two ground state sublevels having a very narrow width Γ', much smaller than the natural width Γ of the excited state. For appropriate laser configurations, the sensitivity of such stimulated Raman transition to the atomic velocity $v = p/M$ (through the Doppler effect) is much higher

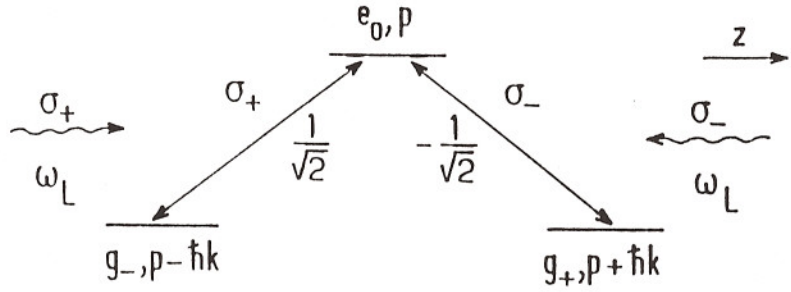

Fig. 6 : Laser configuration and atomic level scheme used in one-dimensional velocity selective coherent population trapping.

than for optical transitions ($kv \sim \Gamma'$ instead of $kv \sim \Gamma$). Such very sensitive momentum-dependent effects are at the basis of two subrecoil cooling schemes which have been demonstrated up to now : velocity selective coherent population trapping (V.S.C.P.T.)[17,18], which is discussed below, and a new scheme using sequences of stimulated Raman and optical pumping pulses, which is described in another paper of this volume[19].

Figure 6 represents the laser configuration and the level scheme used in V.S.C.P.T. Since such a cooling scheme can lead to very large de Broglie wavelengths, atoms can become delocalized in the laser waves, and a full quantum treatment of both internal and external degrees of freedom is required. Fig. 6 shows two counterpropagating laser beams along the $0z$ axis, with σ^+ and σ^- polarizations, driving respectively the $g_{-1}, p - \hbar k \longleftrightarrow e_0, p$ and the $g_{+1}, p + \hbar k \longleftrightarrow e_0, p$ transitions between the three atomic sublevels e_0, g_{-1}, g_{+1} of a $J_g = 1 \longleftrightarrow J_e = 1$ transition, with angular momenta along $0z$ equal to 0, $-\hbar$, $+\hbar$, respectively (e_0, p represents a state where the atom is in the excited sublevel ϵ_0, with momentum p along $0z$). Note the selection rules resulting from the conservation of the total linear and angular momentum along $0z$. The Clebsch-Gordan coefficients of the two σ^+ and σ^- transitions are equal to $+1/\sqrt{2}$ and $-1/\sqrt{2}$, respectively.

Consider now the two orthogonal linear combinations of $|g_{-1}, p - \hbar k\rangle$ and $|g_{+1}, p + \hbar k\rangle$,

$$|\psi_{NC}(p)\rangle = \frac{1}{\sqrt{2}} \left[|g_{-1}, p - \hbar k\rangle + |g_{+1}, p + \hbar k\rangle\right] \tag{10.a}$$

$$|\psi_C(p)\rangle = \frac{1}{\sqrt{2}} \left[|g_{-1}, p - \hbar k\rangle - |g_{+1}, p + \hbar k\rangle\right] \tag{10.b}$$

From the Clebsch-Gordan coefficients of Fig. 6, one can show that :

$$V_{AL} \, |\psi_{NC}(p)\rangle = 0 \tag{11}$$

$$V_{AL} \, |\psi_C(p)\rangle = \frac{\hbar \Omega_1}{2} \, |e_0, p\rangle \tag{12}$$

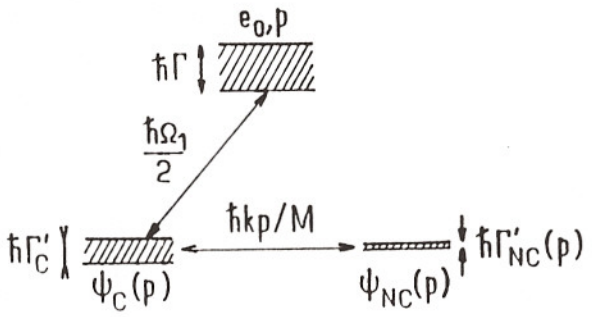

Fig. 7 : Various couplings between the three states $|e_0, p\rangle$, $|\psi_C(p)\rangle$ and $|\psi_{NC}(p)\rangle$, and radiative widths resulting from these couplings.

where V_{AL} is the atom-laser interaction Hamiltonian, and where Ω_1 is the Rabi frequency associated with each wave. The two absorption amplitudes from $g_{-1}, p - \hbar k$ to e_0, p and from $g_{+1}, p + \hbar k$ to e_0, p interfere destructively for $|\psi_{NC}(p)\rangle$, which is thus a non coupled state. The total hamiltonian of the system contains also the kinetic energy term, $P^2/2M$ (we assume that there is no applied magnetic field and that g_{-1} and g_{+1} have the same internal energy). A simple calculation gives :

$$\langle \psi_C(p)| P^2/2M |\psi_{NC}(p)\rangle = \hbar kp/M \tag{13}$$

which shows that $|\psi_C(p)\rangle$ and $|\psi_{NC}(p)\rangle$ are coupled by $P^2/2M$ (motional coupling).

Figure 7 represents the various couplings which exist between the three states $|e_0, p\rangle$, $|\psi_C(p)\rangle$, $|\psi_{NC}(p)\rangle$, and the radiative widths which result from these couplings. In the absence of laser, e_0 is the only radiatively unstable state with a width Γ (natural width). Because of the contamination induced by V_{AL} between $|\psi_C(p)\rangle$ and $|e_0, p\rangle$, $|\psi_C(p)\rangle$ gets a small width Γ'_C, which can be interpreted as the photon absorption rate from the coupled state $|\psi_C(p)\rangle$. When $p = 0$, the non coupled state is completely isolated from the other states. An atom prepared in $|\psi_{NC}(p = 0)\rangle$ remains there indefinitely, so that $|\psi_{NC}(p = 0)\rangle$ is a perfectly trapping state. As soon as p is non zero, the contamination of $|\psi_{NC}(p)\rangle$ by $|\psi_C(p)\rangle$, due to the motional coupling (13), transfers to $|\psi_{NC}(p)\rangle$ a small part, $\Gamma'_{NC}(p)$, of the radiative width Γ'_C pf $|\psi_C(p)\rangle$. The smaller p, the smaller $\Gamma'_{NC}(p)$. The states $|\psi_{NC}(p)\rangle$, with $p \neq 0$, are therefore imperfect traps, which become more and more perfect when $p \longrightarrow 0$. As mentioned above, the sensitivity of this velocity selection mechanism is determined by the ratio $(\hbar kp/M)/\hbar\Gamma'_C$, i.e. by the ratio between the Doppler effect kv and the radiative width Γ'_C of the ground state.

The previous mechanism allows one to select atoms with $p \simeq 0$ and to prevent them from absorbing light and thus from undergoing a random momentum kick due to spontaneous emission. In order to achieve cooling, one must also increase the density of atoms near $p = 0$. This is achieved through optical pumping in momentum space. Due to the random recoil following spontaneous

emission, atoms can be transferred from the $p \neq 0$ absorbing states, into the $p \simeq 0$ trapping states where they pile up. For a given interaction time Θ, one can define a momentum width δp by :

$$\Gamma'_{NC}(\delta p)\Theta \simeq 1 \tag{14}$$

Atoms prepared in $|\psi_{NC}(p)\rangle$ with $|p| \ll \delta p$ will remain trapped in these states during the whole interaction time, while other atoms will have time to undergo fluorescence cycles bringing them in these non absorbing states. Equation (14) gives $\delta p \sim 1/\sqrt{\Theta}$, which shows that the temperature should vary as $1/\Theta$ and is limited only by the interaction time. Such a cooling scheme is quite different from the other ones. It is not based on a friction force but on a velocity selection by quantum interference effects combined with momentum diffusion. It works for any detuning. It has been demonstrated experimentally[17], at one dimension, for the transition $2^3S_1 \longleftrightarrow 2^3P_1$ of metastable Helium atoms at 1.08 μm. Temperatures of $2\mu K$, smaller than the $4\mu K$ recoil temperature $T_R = E_R/kB$ of this transition have been measured, corresponding to a de Broglie wavelength of 1.4 μm larger than the laser wavelength of 1.08 μm.

Extensions of this subrecoil cooling scheme to two or three dimensions have been proposed[18,20,21]. Transitions other than $J_g = 1 \longleftrightarrow J_e = 1$ have been also considered[22], as well as schemes combining velocity selective coherent population trapping and friction forces[23]. Experiments are in progress for 2 dimensional sub-recoil cooling of trapped He atoms, with an interaction time long enough, so that one can hope to reach the nanokelvin range.

QUANTUM JUMP APPROACH TO V.S.C.P.T.

We present now a new theoretical approach to describe the sequence of photon scattering processes occurring in a laser cooling experiment. Similar Monte-Carlo approaches have been recently proposed for dealing with dissipative processes in quantum optics. They are reviewed in another paper of this volume[24]. We take here a specific example, which is the one-dimensonial velocity selective coherent population trapping scheme, introduced in the previous section, and we follow the presentation of ref. 25.

Between two successive spontaneous emission events, the system evolves in a three-dimensional manifold $\mathcal{F}(p)$ formed by the three states $\{|e_0, p\rangle, |g_{\pm 1}, p \pm k\rangle\}$, or equivalently $\{|e_0, p\rangle, |\psi_C(p)\rangle, |\psi_{NC}(p)\rangle\}$. Such an evolution can be described in terms of absorption, stimulated emission and stimulated Raman processes. Since the amplitude for the system to be in e_0 decays with a rate $\Gamma/2$, one can show that the evolution within $\mathcal{F}(p)$ is governed by an effective non Hermitian Hamiltonian H_{eff} obtained by adding, in the projection of the total hamiltonian H onto $\mathcal{F}(p)$, an imaginary part $-i\hbar\Gamma/2$ to the energy of e_0[26].

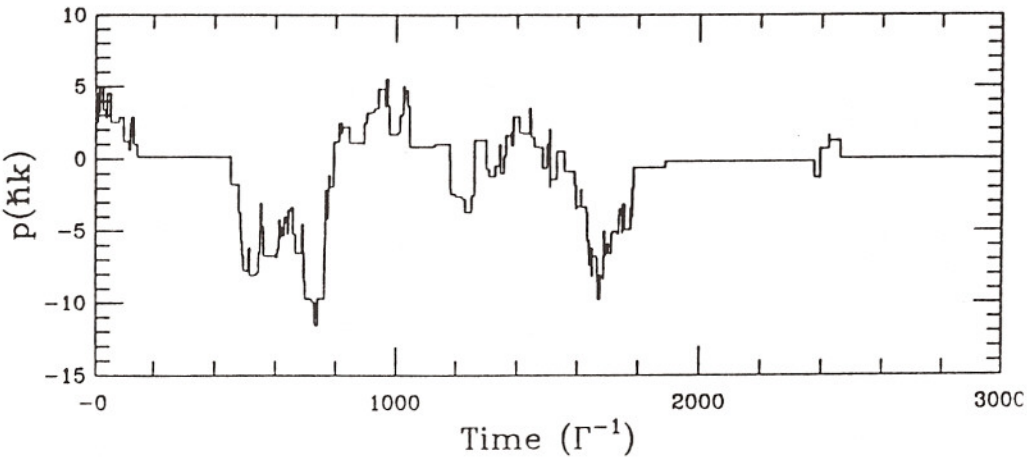

Fig. 8 : Monte-Carlo simulation of the sequence of quantum jumps occurring in velocity selective coherent population trapping.

Spontaneous emission is the dissipative process which introduces a random character in the atomic evolution. At random times, the atom "jumps" from the excited state e_0 into the lower states $g_{\pm 1}$, while a fluorescence photon appears in one of the initially empty modes of the quantized radiation field. Since the fluorescence photon can be emitted in a random direction, the atomic momentum changes in a random way after each jump. The atomic evolution thus appears as a sequence of coherent evolutions within manifolds $\mathcal{F}(p)$, separated by quantum jumps occurring at random times and during which the atom moves from one manifold $\mathcal{F}(p)$ to another one $\mathcal{F}(p')$ determined by the momentum carried away by the fluorescence photon.

It is possible to make a statistical analysis of this sequence of quantum jumps by solving the Schrödinger equation associated with the effective Hamiltonian H_{eff} and by calculating from this solution the "delay function" giving the distribution of the time intervals between two *successive* spontaneous emission processes. Such a method has been already introduced[27,28] for analyzing the "intermittent fluorescence" which can be observed on a single three-level trapped ion. Figure 8 gives the result of a Monte-Carlo simulation of the sequence of quantum jumps occurring in velocity selective coherent population trapping[25]. Each vertical discontinuity corresponds to a quantum jump during which p changes abruptly. Between two successive spontaneous emissions, we have a coherent evolution within $\mathcal{F}(p)$ and p remains constant. It clearly appears in Fig. 8 that the length of the "dark periods" (corresponding to coherent evolutions without any fluorescence photon) increases when p gets closer to zero. Such a result is easy to understand. It means that, when p is close to zero, there is in $\mathcal{F}(p)$ a state in which the atom can remain trapped for a long time. One of the three eigenvalues of H_{eff} has an imaginary part which tends to zero when p tends to zero, and which is actually the width $\Gamma'_{NC}(p)$ introduced in Fig. 7. This gives rise to a long tail in the delay function and results in the fact that one can then wait a long time before observing a fluorescence photon.

Such a Monte-Carlo simulation of the time evolution of the system preserves the quantum features of the problem. Averaging over a set of simulations, one can reconstruct the atomic momentum distribution obtained from the full quantum optical Bloch equations. We get in this way a new insight in the solution of optical Bloch equations from an analysis of what happens to a single atom. Note also that such an approach provides a simple interpretation of the filtering process by which the trapping state $|\psi_{NC}(p)\rangle$ becomes populated. Between two successive spontaneous emission processes, the state of the system is described by a normalized state vector $|\psi(t)\rangle$ given by the solution of the Schrödinger equation corresponding to the Hamiltonian H_{eff} [(*)]. The three eigenstates of H_{eff} have different lifetimes, and if no spontaneous emission has occurred after a time on the order of Γ^{-1} or $(\Gamma'_C)^{-1}$, the weight of $|\psi_{NC}(p)\rangle$, which has a much longer lifetime $(\Gamma'_{NC})^{-1}$, becomes predominant in $|\psi(t)\rangle$.

CONCLUSION

In conclusion, one can sum up the main results which have been recently obtained concerning quantum effects observable on laser cooled atoms.

Thanks to the efficiency of Sisyphus cooling, quantization of atomic motion in an optical potential well has been observed. Evidence has been obtained for well resolved discrete vibrational levels $|v\rangle$, a large fraction of atoms being put in minimum uncertainty states $v = 0$. Using such a basis of discrete states $\{|v\rangle\}$, it is possible to derive universal laws for the temperature. Experimental signals indicate also a large scale spatial order of atoms presenting some analogy with an antiferromagnetic medium.

In these experiments, the laser light plays a triple role : it cools the atoms, traps them in optical potential wells associated with light shifts and probes the internal and external state of the atoms. Note that the description of laser cooling in terms of optical pumping transitions between discrete vibrational levels (see eq. (9)) is quite analogous to the one given for laser cooling of trapped ions[29], except that the trapping of ions is achieved by external static or RF fields and not by the laser light. Reciprocally, it has been recently suggested to extend Sisyphus cooling to trapped ions and temperatures much lower than those obtained by Doppler cooling have been predicted[30].

The high sensitivity of Raman transitions to the Doppler effect provides efficient velocity selection and subrecoil cooling mechanisms. Atom have been cooled below the recoil temperature $T_R = E_R/k_B$, and become delocalized in the laser wave, with a de Broglie wavelength larger than the laser wavelength. They can be prepared in non classical entangled external-internal states (see

---

(*) Such a quantum description of the state of the system between two jumps clearly distinguishes the simulation presented here from a classical Monte-Carlo simulation.

eq. (10a)).

Monte-Carlo simulations of the cooling process preserving the quantum features are possible, in terms of wave function evolutions separated by quantum jumps occurring at random times. These new theoretical approaches provide new physical insights in quantum dissipative processes.

REFERENCES

1. See, for example, Laser Manipulation of Atoms and Ions, Varenna Summer School, 1991, eds. E. Arimondo and W.D. Phillips (North-Holland, Amsterdam, 1992).
2. See, for example, the papers of S. Chu, J. Mlynek, D. Pritchard and F. Shimizu.
3. C. Cohen-Tannoudji, J. Dupont-Roc and G. Grynbert, Processus d'interaction entre photons et atomes (InterEditions et Editions du CNRS, Paris, 1988). English translation : Atom-Photon Interactions. Basic Processes and Applications (Wiley, New-York, 1992), Chap. VI.
4. J.P. Barrat and C. Cohen-Tannoudji, J. Phys. Rad. 22, 329 and 443 (1961).
5. C. Cohen-Tannoudji, Thesis, Paris (1962), Ann. Phys. 7, 423 and 469 (1962).
6. C. Cohen-Tannoudji, C.R. Acad. Sci. 252, 394 (1961).
7. M. Arditi and T.R. Carver, Phys. Rev. 124, 800 (1961).
8. For a review of these developments, see C. Cohen-Tannoudji and W.D. Phillips, Physics Today, 33 (October 1990) and references therein.
9. J. Dalibard and C. Cohen-Tannoudji, J.O.S.A. B6, 2023 (1989).
10. P.J. Ungar, D.S. Weiss, E. Riis and S. Chu, J.O.S.A. B6, 2058 (1989).
11. C. Salomon, J. Dalibard, W.D. Phillips, A. Clairon and S. Guellati, Europhys. Lett. 12, 683 (1990).
12. Y. Castin, J. Dalibard and C. Cohen-Tannoudji, Proceedings of Light Induced Kinetic Effects, L. Moi et al eds, (ETS Editrice, Pisa, 1991).
13. Y. Castin and J. Dalibard, Europhys. Lett. 14, 761 (1991).
14. Y. Castin Thesis, Paris, 1992.
15. P. Verkerk, B. Lounis, C. Salomon, C. Cohen-Tannoudji, J.Y. Courtois and G. Grynberg, Phys. Rev. Lett. 68, 3861 (1992).
16. P.S. Jessen, C. Gerz, P.D. Lett, W.D. Phillips, S.L. Rolston, R.J.C. Spreeuw and C.I. Westbrook, Phys. Rev. Lett. 69, 49 (1992).

During the Conference, other experiments looking for similar effects and

giving preliminary results have been mentioned, at one dimension (H. Metcalf, private communication, and at two dimensions (A. Hemmerich and T.W. Hänsch, private communication).

17. A. Aspect, E. Arimondo, R. Kaiser, N. Vansteenkiste and C. Cohen-Tannoudji, Phys. Rev. Lett., 61, 826 (1988).
18. A. Aspect, E. Arimondo, R. Kaiser, N. Vansteenkiste and C. Cohen-Tannoudji, J.O.S.A. B6, 2112, (1989).
19. See the paper of S. Chu in this volume.
20. F. Mauri, F. Papoff and E. Arimondo, Proceedings of Light Induced Kinetic Effects, L. Moi et al eds, (ETS Editrice, Pisa, 1991).
21. M.A. Ol'shanii and V.G. Minogin, Proceedings of Light Induced Kinetic Effects, L. Moi et al eds, (ETS Editrice, Pisa, 1991).
22. F. Papoff, F. Mauri and E. Arimondo, J.O.S.A. B6, 321 (1992).
23. F. Mauri and E. Arimondo, Europhys. Lett. 16, 717 (1991).
24. See the paper of J. Dalibard in this volume and references therein.
25. C. Cohen-Tannoudji, F. Bardou and A. Aspect, in Laser Spectroscopy X, M. Ducloy, E. Giacobino and G. Camy eds (World Scientific, 1992).
26. See, for example, Ref. 3, Chap. III.
27. C. Cohen-Tannoudji and J. Dalibard, Europhys. Lett. 1, 441 (1986).
28. P. Zoller, M. Marte and D.F. Walls, Phys. Rev. A35, 198 (1987).
29. D. Wineland and W. Itano, Phys. Rev. A20, 1521 (1979).
30. D.J. Wineland, J. Dalibard and C. Cohen-Tannoudji, J.O.S.A. B9, 32 (1992).